AIMS Geosciences

AIMS Geosciences, 12(4): 972–997.
DOI: 10.3934/geosci.2026037
Received: 11 May 2026
Revised: 08 August 2026
Accepted: 01 September 2026
Published: 09 October 2026

https://www.aimspress.com/journal/geosciences

Research article

Modeling flood susceptibility using frequency ratio and Shannon's entropy models: Ghataprabha Basin, India

Uttam Pawar[1], Kumudu Madhawa Kurugama[2] Upaka Rathnayake[3,*]and Nitin Muttil[4,5]

[1] Department of Geography, Shri Bhausaheb Vartak Arts, Commerce, and Science College, Borivali (West), Mumbai-400 091, (Maharashtra), India
[2] Department of Civil and Environmental Engineering, Tohoku University, Sendai, Japan
[3] Department of Civil Engineering and Construction, Faculty of Engineering and Design, Atlantic Technological University, Sligo, F91 YW50, Ireland
[4] School of Advanced Engineering, UPES, Dehradun, Uttarakhand, 248007, India
[5] Institute for Sustainable Industries & Liveable Cities, Victoria University, P.O. Box 14428, Melbourne, VIC, 8001, Australia

* **Correspondence:** Email: upaka.rathnayake@atu.ie; Tel: +353-899-460-732; Fax: +353-71-916-0475.

Abstract: Floods are catastrophic events that adversely influence the population in the Ghataprabha Basin, India. Therefore, the objective of this research was to create a flood susceptibility map (FSM) utilizing the Frequency Ratio (FR) and Shannon's Entropy (SE) models. Eleven flood-controlling factors, namely, slope, elevation, aspect, Topographic Wetness Index, Stream Power Index, rainfall, distance from rivers, drainage density, soil types, land use/land cover, and distance from roads, were used in the analysis. Among the 191 flood locations, 70% (134) were used for model training, and 30% (57) for testing. Furthermore, a Pearson's correlation analysis was conducted to examine the interrelationships among flood-controlling factors and the impact of each factor on the accuracy of the final map. The SE model indicated that the most significant factors influencing floods were built-up area (2.60), stream density (0.70), soil type (0.44), rainfall (0.35), and distance from streams (0.33). The area under the curve (AUC) indicated that the SE model achieved higher success (84.99%) and prediction (84.89%) rates than the FR model. The AUC analysis confirmed the SE model's superiority over the FR model. The reliability and accuracy of the SE model's results are crucial for flood disaster management and planning in the Ghataprabha Basin.

Keywords: Ghataprabha Basin; flood susceptibility; flood risk; frequency ratio; Shannon's Entropy

1. Introduction

Floods are natural and manmade disasters that cause annual human, economic, and environmental losses [1]. With increasing frequency and severity, floods have become a significant global concern, distressing populations and destroying infrastructure [2,3]. According to statistics, about 23% of the global population is at risk of flooding, with low- and middle-income countries disproportionately affected [4]. The application of flood-mitigation measures, such as identifying flood hazard zones, producing flood-risk zone maps, implementing early warning systems, and maintaining risk databases, can help moderate flood impacts [5]. Flood susceptibility maps (FSMs) help identify flood-prone regions, enabling more informed decision-making in urban planning and disaster management [6,7]. Globally, the importance of flood prevention has been recognized through frameworks (Sendai Framework), which emphasize increasing access to disaster risk information [8].

Saleh et al. [9] stated that numerous novel methods have been developed and applied for the FSM, ranging from process-based numerical models to machine learning and statistical techniques. Popular hydrodynamic models such as HEC-RAS [10], TELEMAC-2D [11], and MIKE URBAN [12] solve complex numerical equations, including the shallow-water equations, to accurately simulate rainfall-runoff processes. While these models effectively depict physical processes, they require extensive calibration, sensitivity analysis, and significant processing time. Furthermore, the application of such models is often limited by data availability and reliability, especially over large areas [1]. Moreover, the Analytical Hierarchy Process and the Analytical Network Process have gained popularity for their simplicity [13,14]. These approaches allow the integration of expert knowledge to evaluate flood risk factors but are prone to subjectivity and bias. In contrast, machine learning models, such as Support Vector Machine [15], Random Forest [16], decision-tree-based boosting models [7], and Artificial Neural Networks [17], have demonstrated higher predictive accuracy for flood susceptibility mapping. Despite their success, machine learning models are often seen as "black boxes" due to their complexity and lack of transparency, which reduces their appeal to stakeholders who seek interpretability in decision-making [18].

When advanced models, for example, process-based numerical models and those based on soft computing and machine learning, are limited by the need for high-resolution spatial data and sophisticated computing infrastructure, statistical models become highly valuable due to their reliance on more straightforward datasets, such as historical flood records and digital elevation models (DEMs) [19]. Statistical techniques are frequently used in FSM due to their simplicity and speed compared to more complex methods such as machine learning [20]. These approaches are particularly well-suited for disaster mapping because they are easier to interpret and can process data quickly. Statistical techniques include Weight of Evidence, Frequency Ratio (FR), Shannon's Entropy (SE), Evidential Belief Function, Statistical Index, and Certainty Factor [5,21–24]. These methods enable more comprehensive analysis by accounting for the combined effects of multiple variables. Furthermore, various Machine Learning (ML) algorithms have been employed to identify areas prone to flooding. The ML techniques, such as Support Vector Model (SVM) [25–27], Artificial Neural Networks (ANN) [28], Convolutional Neural Networks (CNN) [27], Decision Tree (DT) [29], Random Forest (RF) [29–31], Adaptive Network-Based Fuzzy Inference System (ANFIS) [32],

Gradient Boosting (GB) [31], and Extreme Gradient Boosting (XGBoost) [30,31], successfully identified areas that experienced flooding.

India has been ranked among the ten countries most impacted by floods in the Asia-Pacific region, with approximately 7.17 million hectares affected annually. This leads to the destruction of 1.2 million homes, the loss of 1,654 human lives, 618,248 cattle, and an annual economic loss of Rs 5,649 crores [33]. Our prime objective of this research is to identify flood-prone zones in the Ghataprabha Basin using the FR and SE models. Additionally, efforts have been made to evaluate the influence of various flood-controlling factors (FCF) and identify correlations among them, enabling a user-friendly, efficient analysis process.

1.1. Study areas

The Ghataprabha Basin is one of the sub-basins of the Krishna Basin (Figure 1a). It covers parts of Maharashtra and Karnataka (Figure 1b). The drainage basin area of the Ghataprabha is 8,829 km^2 [34]. The Ghataprabha River is one of the tributaries in the upper Krishna Basin and originates at an altitude of 884 m (MSL) near Chaukul village in Sindhudurg district of Maharashtra (Figure 1c). It flows about 283 km eastward before joining the Krishna River near Chikksangam, in Karnataka [34]. The major tributaries of the Ghataprabha are the Hiranyakeshi, Tamrapani, and Markandeya rivers (Figure 1c). The Ghataprabha Basin extends between 15 °N and 16° 25 ′N latitudes and from 70 °E to 75° 55 ′E longitudes (Figure 1c). According to Pathak and Dodamani [35], the Ghataprabha basin experiences temperatures ranging from 7 °C in winter to 41 °C in summer. In the Ghataprabha Basin, the annual average rainfall ranges from 646 mm in Vijaypura to 3212 mm in Sindhudurg. Rainfall variability within the basin ranges from 20% to 25%. Vijaypura district has the lowest recorded annual average rainfall, whereas Sindhudurg district has the highest (Table 1). Overall, the mean annual rainfall in the Ghataprabha Basin is 1683 mm, with an average variability of 24% (Table 1). Most of the Ghataprabha Basin lies on the Deccan Traps, except for the central and southern portions, which are underlain by the Kaladgi and Dharwad supergroups (Figure 2).

Table 1. Summary of the annual average rainfall of the Ghataprabha Basin.

District/Rainfall	Minimum (mm)	Maximum (mm)	Mean (mm)	Standard Deviation (mm)	Coefficient of Variability (%)
Sindhudurg	1876	4282	3212	659	20
Kolhapur	798	3451	2102	438	21
Belagavi	561	2853	1685	450	27
Bagalkot	362	1414	772	197	25
Vijaypura	320	1121	646	160	25
Ghataprabha Basin	783	2624	1683	381	24

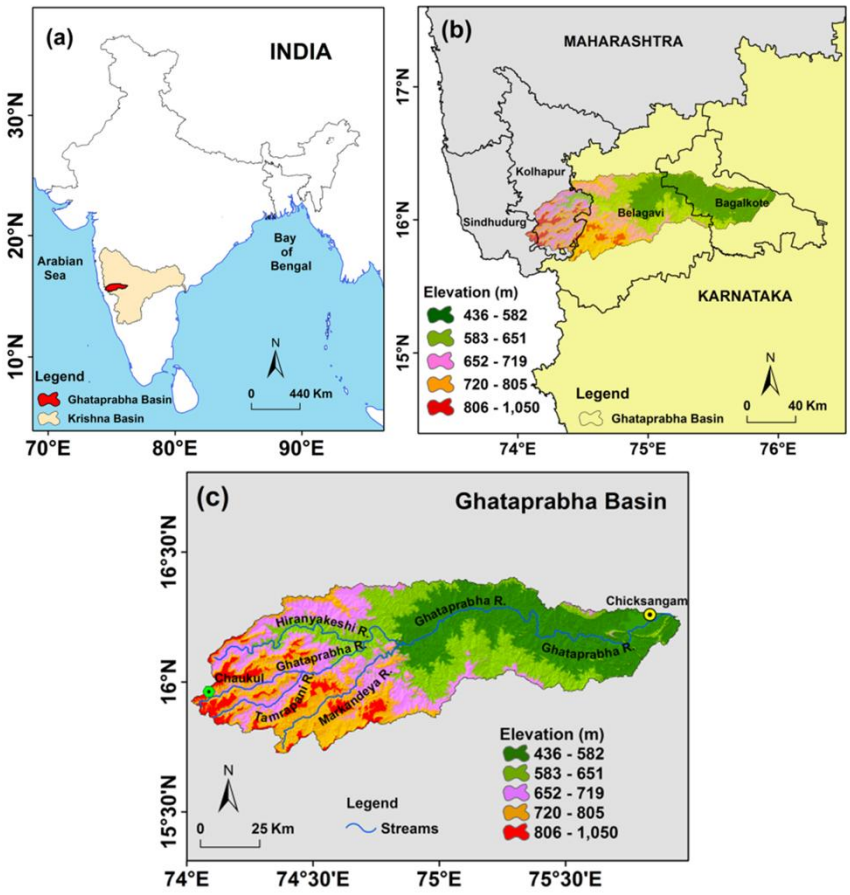


Figure 1. Location map and network of main streams in the Ghataprabha Basin.

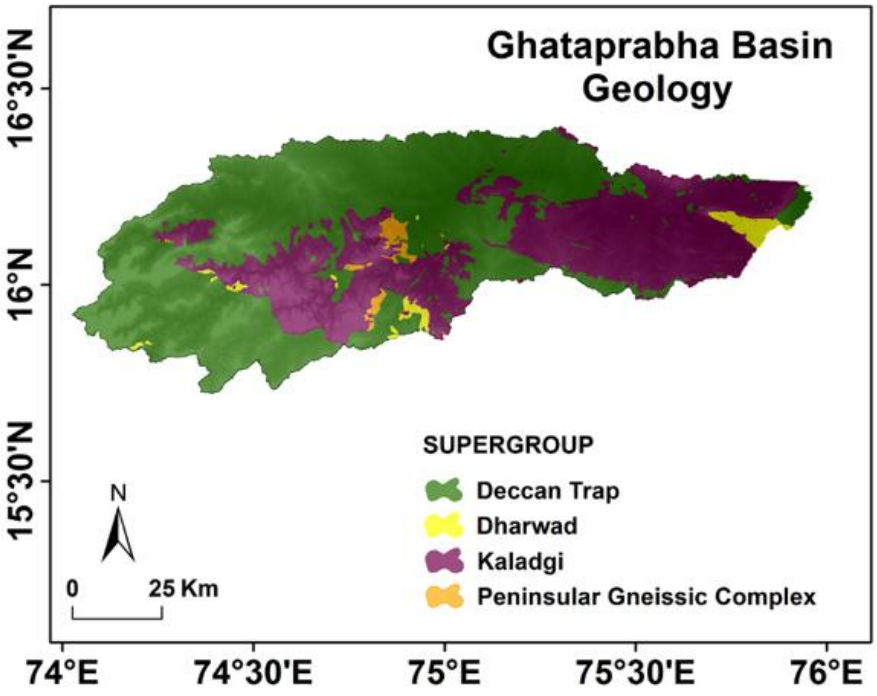


Figure 2. Geology of the Ghataprabha Basin.

2. Materials and methods

The flood susceptibility analysis (FSA) study was conducted for the Ghataprabha Basin using the data shown in Table 2. The natural break (Jenks) classification method was used to reclassify all selected FCFs for the FR and SE model analyses after they were transformed into raster maps and resampled to a 30 m resolution in ArcGIS 10.1 [5,36–38]. Flood inventory, determination of FCFs, and flood modeling and validation are steps in the FSA in the Ghataprabha Basin (Figure 3).

Table 2. Summary of flood controlling factors, data sources, data type, and map layers.

Dataset	Data Types	Source	Derived map layers
ASTER DEM (30m*30m)	Raster grid and Vector (polyline)	https://earthexplorer.usgs.gov (accessed on 12 January 2024)	Elevation, Slope, Aspect, Curvature, TWI, SPI, Stream density, and distance from streams
Rainfall	Attribute data	https://www.indiawaterportal. org/ met_ data (accessed on 25 January 2024)	Rainfall map
Soil types	Vector data (Polygon)	http://www.fao.org (accessed on 25 January 2024)	Soil map
LULC	Vector data (Polygon)	https://gee-community catalog.org/projects/S2TSLULC/ (accessed on 12 January 2024)	Landuse/Landcover (LULC) map
Distance from roads	Vector data (Polyline)	https://www.diva-gis.org/datadown (accessed on 12 January 2024)	Road map
Flood Data	Vector data (Point)	Government reports and Newspapers	Flood inventory map

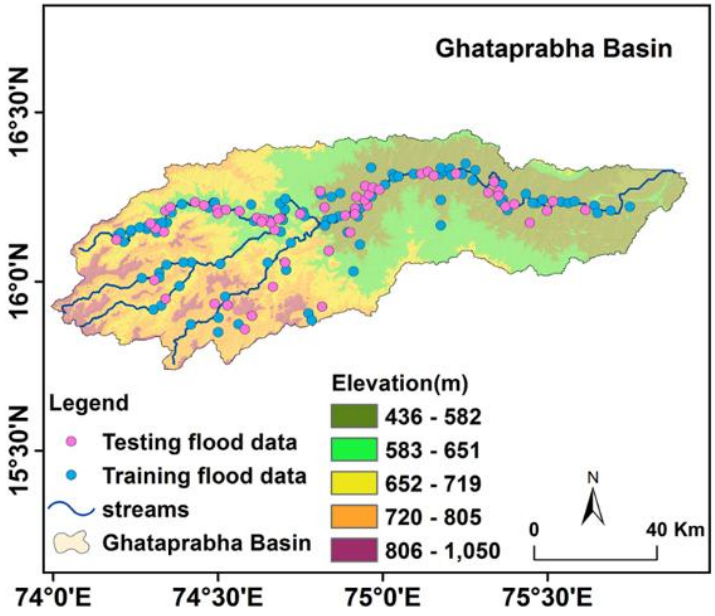


Figure 3. Flood inventory map of the Ghataprabha Basin.

2.1. Flood inventory mapping

The precision of the FSM is highly dependent on the availability of detailed records of previous flood events [39]. The flood inventory map of the Ghataprabha was created in ArcGIS using 191 flood locations identified from the flood that occurred from August 8–10, 2019. The flood location information was gathered from government reports and newspapers (Table 2). The flood locations were marked on Google Earth and exported as point data. The flood location records were divided into two parts: one for calibration and the other for validation [40]. Accordingly, flood data were arbitrarily split into 70% for training and 30% for model testing and model validation [5,41]. The FR and SE models were thus trained (tested) with 134 (57) flood data (Figure 4).

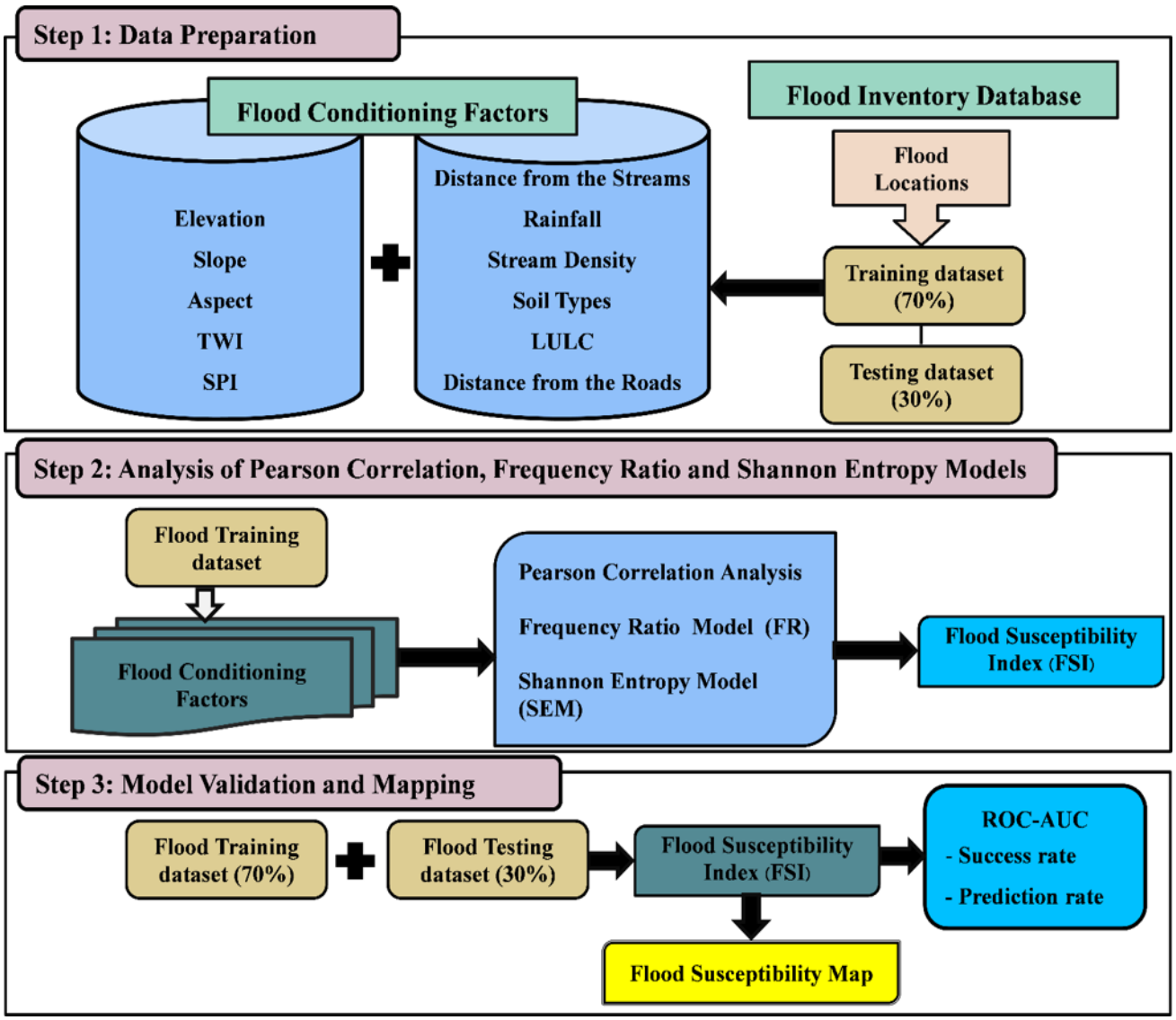


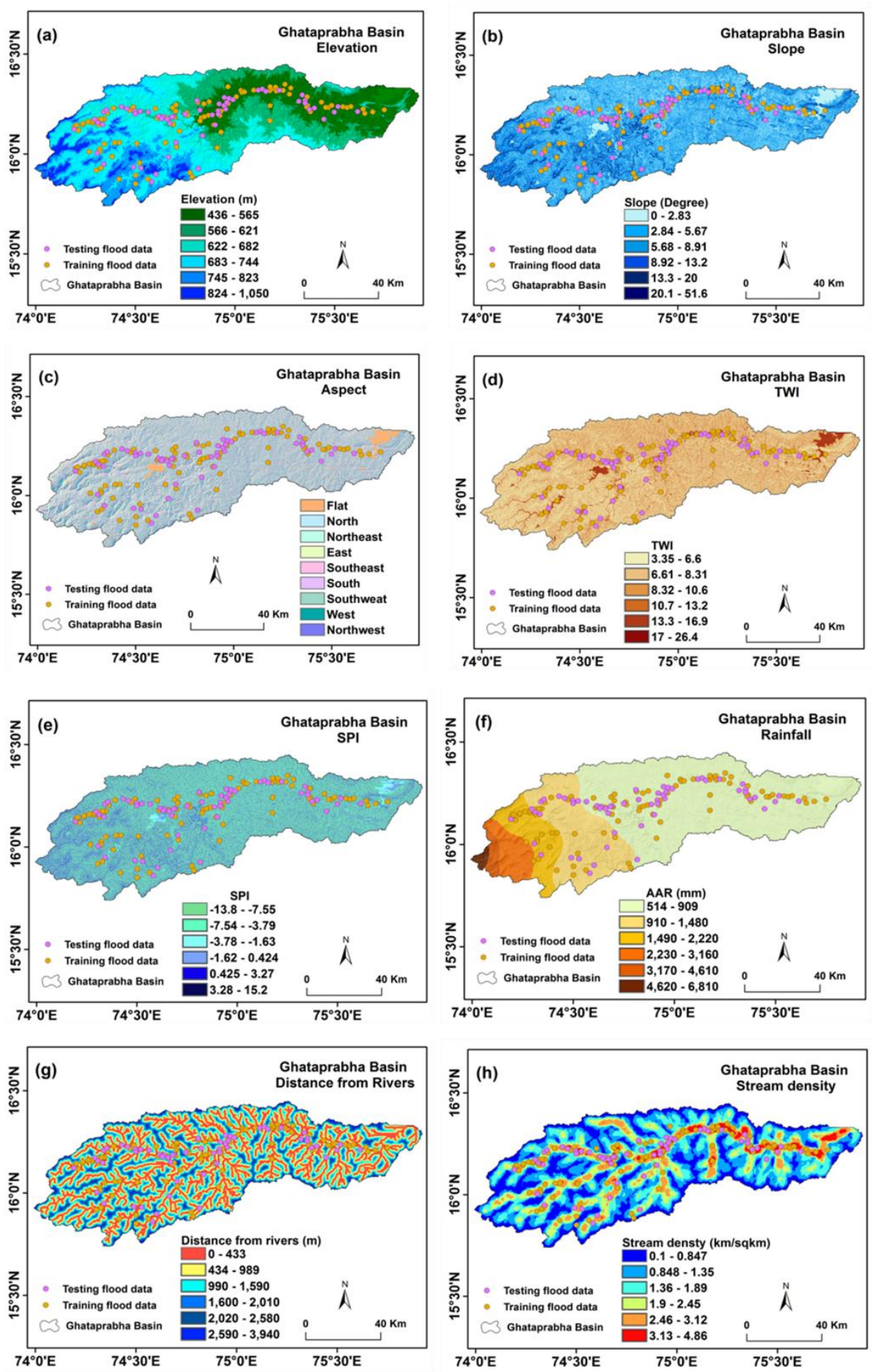
Figure 4. Flowchart of the research methodology.

2.2. Flood controlling factors

The FSA and mapping of flood-susceptible areas in the Ghataprabha Basin were performed using 11 conditioning factors, as depicted in Figure 5. Elevation and slope are the most effective factors in generating surface runoff and the magnitude of flooding in the basin after a precipitation event [5,42]. The maximum elevation (1050 m) is observed in the western part of the basin and decreases steadily toward the east to 436 m, where the Ghataprabha joins the Krishna River (Figure 5a). Besides, the slope of the basin varies from 0 ° to 51.6 ° (Figure 5b). Generally, a region with a flat surface and low slope has a higher probability of flooding than regions at higher altitudes and with steeper slopes [43]. According to Bathrellos et al. [44], the land aspect (slope direction) is another noteworthy FCF in flood analysis. Aspect is the orientation of a slope, usually measured in degrees from north [45]. The west and southwest parts of the Ghataprabha Basin experience heavy rain in the monsoon season (Figure 5c). The TWI indicates the flow capacity that can be accommodated at a location in the basin and the water's propensity to move downslope [46]. SPI is the rate of surface runoff's erosive power at a particular location within a river basin [47]. TWI values ranged from 3.35 to 26.4 (Figure 5d).

SPI values in this analysis ranged from −13.8 to 15.2 (Figure 5e). The rainfall distribution map of the Ghataprabha Basin was created using GIS software. The AAR varied from 6810 to 514 mm in the basin (Figure 5f). Here, we considered the distance from the river as one of the FCFs and created a map using ArcGIS. The map showed the maximum distance of 3940 m from the river channels (Figure 5g). A higher distance from streams indicates a lower flood risk, resulting in fewer fatalities and less displacement. In contrast, a lower numerical value indicates a higher flood risk, which may lead to increased flood-related fatalities and displacements [48]. The term human-flood distance refers to the distance between human settlements and areas affected by flooding during each flood event [48]. A drainage (stream) density map of the Ghataprabha River was created in ArcGIS, revealing a range of 0.1 to 4.86 km/km^2 (Figure 5h). Drainage density is defined as the total length of channels per unit area [49]. Das [50] noted a direct association between drainage density and surface runoff, suggesting that higher drainage density results in increased runoff, consequently exacerbating flooding.

Soil type determines the rates of water infiltration and surface runoff in the basin. Soil texture characteristics affect the volume of rainwater that permeates into subsurface reservoirs and the amount retained in the unsaturated zone [51]. In the Ghataprabha Basin, six soil types have been identified, namely, Plinthic Acrisols (Ap), Vertic Cambisols (Bv), Chromic Luvisols (Lc), Eutric Nitosols Pellic (Ne), Chromic Vertisols (Vc), and Vertisols (Vp) observed in the Ghataprabha Basin (Figure 5i). The primary LULC types in the Ghataprabha Basin include agriculture, urban areas, vegetation, water bodies, open land, and hilly terrain (Figure 5j). The surface runoff that flows from higher to lower elevations in the basin is affected by natural and human-induced factors (vegetation cover and urban areas). According to Alaghmand et al. [52], densely forested regions exhibit the highest rates of infiltration and abstraction. Finally, the distance from the road was calculated in ArcGIS and divided into six groups to determine how far a given pixel was from the closest road line (Figure 5k).


(a)
Ghataprabha Basin
Elevation
Elevation (m)
436 - 565
566 - 621
622 - 682
683 - 744
745 - 823
824 - 1,050
(b)
Ghataprabha Basin
Slope
Slope (Degree)
0 - 2.83
2.84 - 5.67
5.68 - 8.91
8.92 - 13.2
13.3 - 20
20.1 - 51.6
(c)
Ghataprabha Basin
Aspect
Flat
North
Northeast
East
Southeast
South
Southweat
West
Northwest
(d)
Ghataprabha Basin
TWI
TWI
3.35 - 6.6
6.61 - 8.31
8.32 - 10.6
10.7 - 13.2
13.3 - 16.9
17 - 26.4
(e)
Ghataprabha Basin
SPI
SPI
-13.8 - -7.55
-7.54 - -3.79
-3.78 - -1.63
-1.62 - 0.424
0.425 - 3.27
3.28 - 15.2
(f)
Ghataprabha Basin
Rainfall
AAR (mm)
514 - 909
910 - 1,480
1,490 - 2,220
2,230 - 3,160
3,170 - 4,610
4,620 - 6,810
(g)
Ghataprabha Basin
Distance from Rivers
Distance from rivers (m)
0 - 433
434 - 989
990 - 1,590
1,600 - 2,010
2,020 - 2,580
2,590 - 3,940
(h)
Ghataprabha Basin
Stream density
Stream densty (km/sqkm)
0.1 - 0.847
0.848 - 1.35
1.36 - 1.89
1.9 - 2.45
2.46 - 3.12
3.13 - 4.86
Testing flood data
Training flood data
Ghataprabha Basin
N
0
40 Km
74°0'E
74°30'E
75°0'E
75°30'E
16°30'N
16°0'N
15°30'N

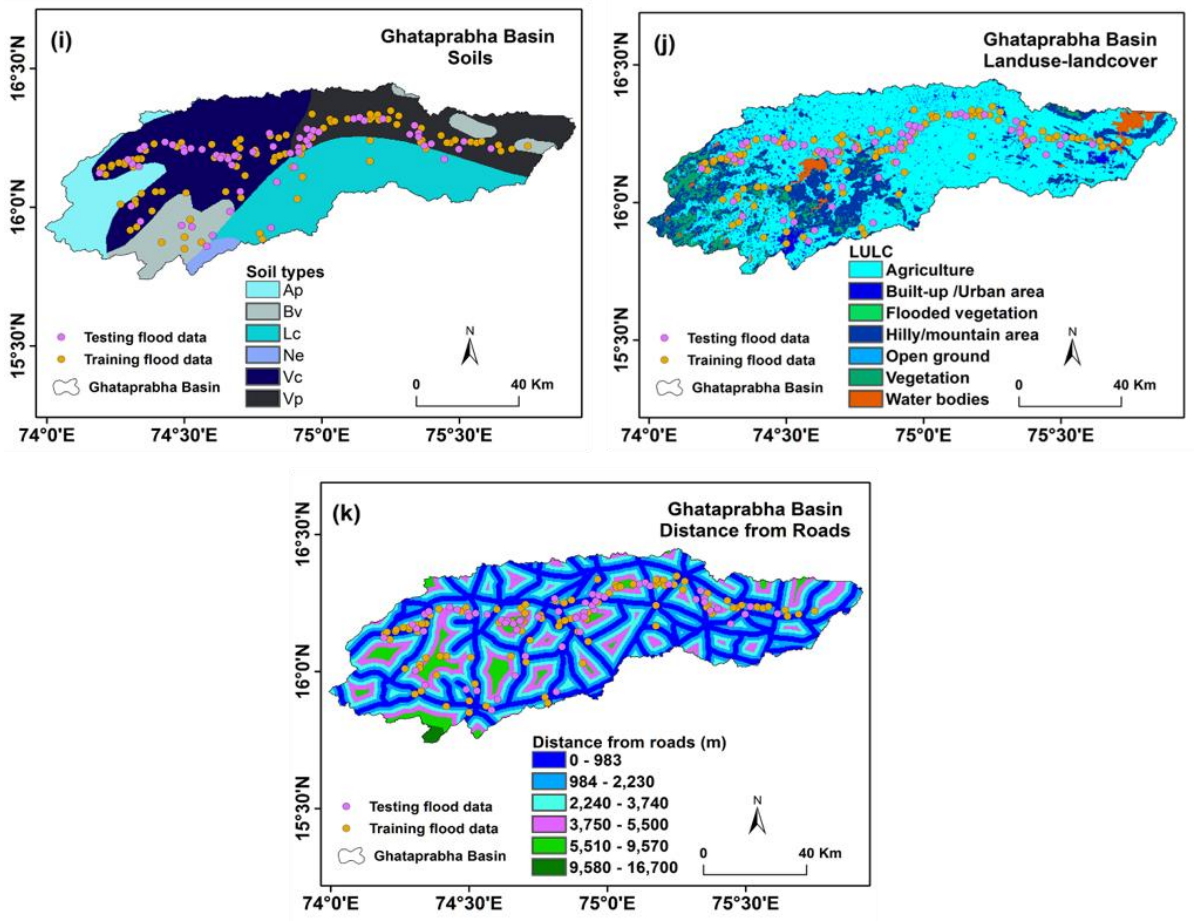


Figure 5. Flood controlling factors: (a) Elevation, (b) Slope, (c) Aspect, and (d) TWI. Flood controlling factors: (e) SPI, (f) Rainfall, (g) Distance from rivers, and (h) Stream density. Flood controlling factors: (i) Soils, (j) LULC, and (k) Distance from Roads.

2.3. Frequency Ratio (FR) model

The FR is the most commonly applied statistical model for susceptibility analysis of natural hazards [53,54]. The flood area and flood-occurrence ratio for every class of the FCF were computed using Equation1.

$$FR_{ij} = \left(\frac{\frac{Nf_{pix_{ij}}}{Nft_{pix_j}}}{\frac{Nc_{pix_{ij}}}{Nct_{pix_{ij}}}} \right) \quad (1)$$

where FR_{ij} shows the FR of the class i of factor j; $Nf_{pix_{ij}}$ is the number of flood pixels within the class i of factor j; $Nft_{pix_{ij}}$ is the total number of flood pixels within the factor j; $Nc_{pix_{ij}}$ is the number of pixels within the class i of factor j; and $Nct_{pix_{ij}}$ is the total number of pixels within the factor j.

Finally, the flood susceptibility index was derived by summing the FR values of all FCFs, as specified in Equation 2.

$$FSI_{FR} = \sum_{j=1}^{n} FR_j \tag{2}$$

where, FSI is the flood susceptibility index; and FR_j represents the frequency ratio for each FCF.

2.4. Shannon's Entropy (SE) model

Shannon [55] introduced the entropy model, which has been used to assess flood susceptibility by quantifying disorder (entropy) in the distributions of explanatory variables for floods [56,57]. The SE model is used to determine the weight of each FCF for flood susceptibility. The final weight assigned to each variable was calculated using the following equations (Equations 3–9).

$$P_{ij} = \frac{b}{a} \tag{3}$$

$$(P_{ij}) = \frac{P_{ij}}{\sum_{i=1}^{S_j} P_{ij}} \tag{4}$$

where, a and b are the domain and flood percentages, respectively, and (P_{ij}) is the probability density of i^{th}class of j^{th} factor.

$$H_j = -\sum_{i=1}^{S_j} (P_{ij})\, log_2(P_{ij}) \;; j = 1,2, \dots, n \tag{5}$$

$$H_{j\,max} = log_2(S_j) \tag{6}$$

$$\frac{H_{j\,max} - H_j}{H_{j\,max}}; I = (0,1) \tag{7}$$

$$P_j = \frac{1}{S_j} \sum_{i=1}^{S_j} P_{ij} \tag{8}$$

$$W_j = I_j \times P_j \tag{9}$$

where H_j and $H_{j\,max}$ represent entropy values and S_j is the number of classes of each conditioning factor, n is the number of conditioning factors, I_j is the information coefficient, and W_j is the weight value attributed to each flood conditioning factor.

Finally, the FSI was calculated using the Equation 10.

$$FSI_{SE} = \sum_{i=1}^{n} \frac{Z}{m_i} \times C \times W_j \tag{10}$$

where i is the total number of controlling factors, Z is the number of classes of the controlling factor that has the most classes, m_i is the number of classes within each specific factor, C is the value of the class after secondary classification, and W_j is the final weight of each factor.

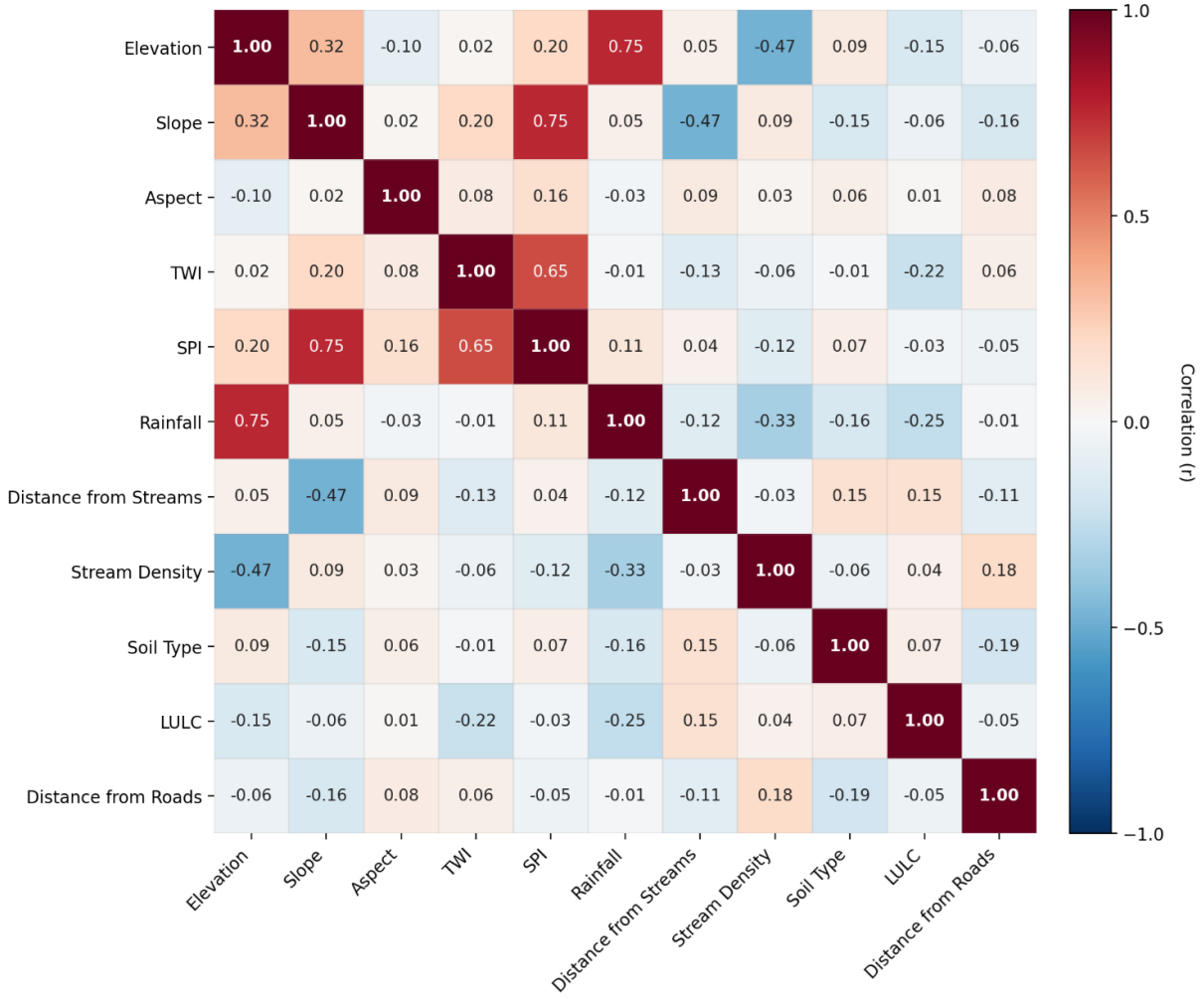


Figure 6. Pearson correlation matrix and the heatmap of flood-controlling factors.

2.5. Model performance evaluation

The Receiver Operating Characteristic (ROC) Curve is a popular method for assessing the effectiveness and validity of prediction models. The predictive capacity of a model can be accurately reflected by its area under the ROC curve (AUC), the most important measure of ROC. As the AUC increases, a model's performance gets better [58]. In this study, the training dataset (70%) was used to create the success rate curve, and the testing dataset (30%) was used to determine the prediction rate curve [5]. The AUC was computed using Equation 11.

$$UC = \sum_{i=0}^{n}(x_i - x_{i-1})y_i - [\frac{(x_i - x_{i-1})(y_i - y_{i-1})}{2}] \quad (11)$$

where, x_i is the percentage of the area and y_i is the flood area.

3. Results and discussions

3.1. Evaluation of the correlation between flood-controlling factors

The Pearson correlation matrix depicted in the heatmap indicates strong positive correlations between elevation and rainfall (r = 0.75), between slope and the stream power index (SPI) (r = 0.75), and a moderate correlation between elevation and slope (r = 0.32) (Figure 6). This reflects the influence of topography on rainfall distribution and runoff generation. The Topographic Wetness Index (TWI) showed strong positive correlations with the stream power index (r = 0.65). Several variables exhibited moderate negative correlations, particularly elevation with stream density (r = −0.47), slope and distance from streams (r = −0.47), and rainfall with stream density (r = −0.33), indicating that higher elevations, steeper slopes, and higher rainfall areas are generally associated with lower stream density in the study region. Likewise, land use and land cover (LULC) and distance from road were weakly negatively correlated (r = −0.05), indicating that developed land tends to be closer to transportation networks. The correlation structure confirms that the selected predictors are appropriate for use in flood susceptibility models, such as the Frequency Ratio and Shannon's Entropy models, and that they exhibit no significant redundancy.

3.2. Flood investigation by the FR model

The FSA for the Ghataprabha Basin was prepared using 11 FCFs, and the outcomes are summarized in Table 3. Generally, an FR value greater than 1 indicates a strong correlation between FCF and flood regions, whereas an FR value less than 1 indicates a weak correlation [59]. According to Tehrany et al. [60], a higher FR represents a robust relationship between FCF and flood. The results of the association between elevation and flood sites indicated that the maximum FR (1.73) was found in the elevation range of 436–565 m, which covered about 43% of the basin area (Table 3). This indicates that lower-elevation regions in the Ghataprabha Basin are more vulnerable to flooding. The FR exceeding 1 was observed for the slopes of 2.84 °–5.67 ° and 8.92 °–13.2 °, respectively. Almost 54% of flood-prone areas were identified in these two slope categories (Table 3). According to Khosravi et al. [61], the zones with lower (higher) slopes have a greater (lesser) chance of flooding. The FR values above 1 were noted for the directions of slopes facing southwest (1.34), west (1.22), east (1.13), and north (1.12). In the TWI analysis, the TWI class 3.35–6.60 has the highest FR (1.30), accounting for 50% of the basin. In the TWI class 3.35–6.60, a total of 67 flood locations were identified (Table 3). According to Moore et al. [46], TWI indicates how topography affects the position and extent of wet zones that create surface runoff, assuming fixed conditions and homogeneous soil characteristics. The highest FR ratio (1.27) was observed for the SPI category, ranging from −13.8 to −7.55, indicating that this range is more vulnerable to flooding, while the minimum (0) was observed for the SPI category, which ranged from −7.54 to −3.79 (Table 3). FR values greater than 1 were observed in the region with AAR ranging from 1481 mm to 2220 mm (FR = 1.52) and from 514 mm to 909 mm (FR = 1.04). However, almost 62% of the catchment area (86 flooded sites) fell within the AAR range of 514 mm to 909 mm, indicating that the low rainfall zone is more vulnerable to flooding (Table 3; Fig.4f). The relationship between distances from rivers showed the maximum FR (2.30) for the distance class 0–433 m. Out of 134 locations, 91 flood sites were within a distance of 0–433 m from the riverbank (Table 3). This revealed that localities near

the riverbed are more exposed to flooding, and the likelihood of flooding decreases with increasing distance from the river [62]. Our findings indicate that greater distance between human settlements and the river leads to a significant decrease in flood-related fatalities and displacements. This finding is consistent with research highlighting that managed retreat from areas susceptible to flooding can reduce the population's exposure to flood risks [5,48,63]. Stream (drainage) density is one of the major FCFs that indicate how a drainage basin will respond to runoff and flooding. The maximum FR (6.05) was noted for the stream density class 3.13–4.86 km/km^2, followed by the stream density class 2.46–3.12 km/sq .km (Table 3). This suggests that stream density directly affects runoff and flood occurrence [64]. The highest FR (4.13) was observed for soil type Bv, indicating that Bv soil contributed to the flood due to its waterlogging characteristics during the rainy season. Additionally, of the 134 localities, 60 flooded sites (45% of the area) were observed in the Bv soil-type zone (Table 3). Moreover, LULC affects runoff and infiltration rates, which influence the timing of flow concentration in a catchment [65]. This study revealed that built-up areas (FR = 18.86) are more prone to flooding due to low infiltration rates and higher runoff rates. Similar observations were noted by Tehrany et al. [60]. The maximum FR (1.51) for distance from the road was observed for the road distance class 5510–9570 m. As the distance from the road increased, the likelihood of flooding decreased [66]. Last, flood susceptibility index values derived from the FR model and the FSM of the Ghataprabha Basin were produced (Figure 7a). The FSM was classified into five flood susceptibility zones: very low, low, moderate, high, and very high [5]. According to the FSM results, 11% of the basin was in the moderate flood susceptibility class, while 2% (3%) was in the extremely high (high) susceptibility classes. Near major rivers, where the surface was flat, there were high- and very-high flood-susceptible zones. Approximately 85% of the basin area was observed in the class of low susceptibility to very low susceptibility to flooding (Figure 7b).

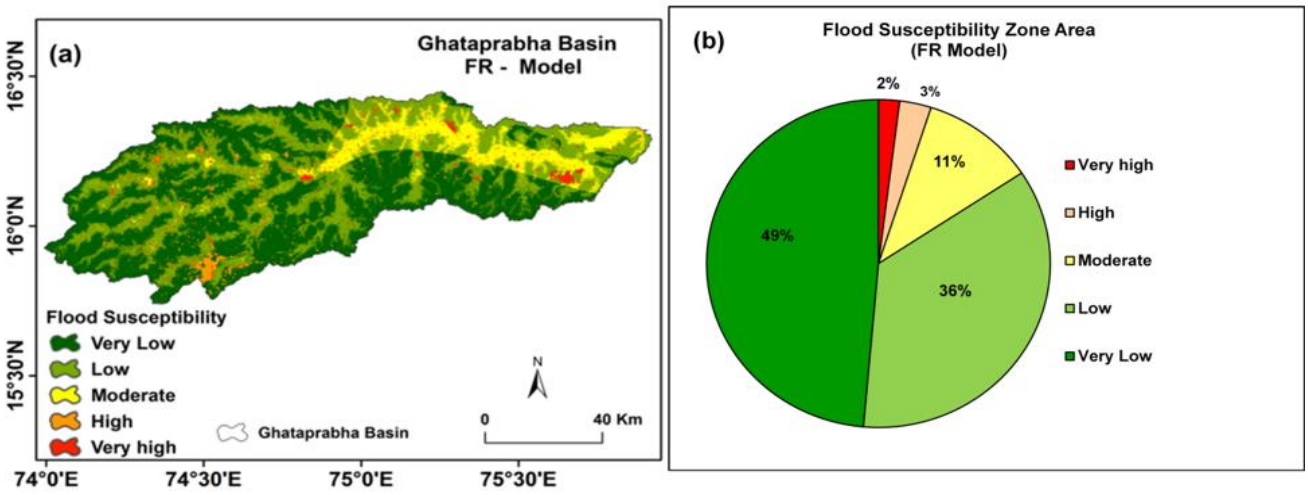


Figure 7. Flood susceptibility results from the FR model.

Table 3. Results of the FR and SE models for various classes of the flood factors.

Factors	Class	Class Pixels	Area (%)	Flood Pixels	Flood Area (%)	FR	(pij)	Hj	Hj max	lj	Pij	Wj
Elevation (m)	436–565	2373670	24.55	57	42.54	1.73	0.37	0.53	2.58	0.21	0.78	0.16
	566–621	1920237	19.86	23	17.16	0.86	0.18	0.45				
	622–682	1958536	20.26	32	23.88	1.18	0.25	0.50				
	683–744	1801000	18.63	20	14.93	0.80	0.17	0.44				
	745–823	1199675	12.41	2	1.49	0.12	0.03	0.14				
	824–1050	413658	4.28	0	0.00	0.00	0.00	0.00				
Slope (degree)	0.0–2.83	3026959	31.31	35	26.12	0.83	0.18	0.44	2.58	0.11	0.79	0.09
	2.84–5.67	3471208	35.91	60	44.78	1.25	0.26	0.51				
	5.68–8.91	1933164	20.00	23	17.16	0.86	0.18	0.45				
	8.92–13.20	852704	8.82	13	9.70	1.10	0.23	0.49				
	13.3–20.0	311464	3.22	3	2.24	0.69	0.15	0.41				
	20.1–51.60	71277	0.74	0	0.00	0.00	0.00	0.00				
Aspect	Flat	1206708	12.48	11	8.21	0.66	0.07	0.27	3.17	0.01	1.01	0.01
	North	1097836	11.36	17	12.69	1.12	0.12	0.37				
	Northeast	1057906	10.94	13	9.70	0.89	0.10	0.33				
	East	1080600	11.18	17	12.69	1.13	0.13	0.38				
	Southeast	1189031	12.30	17	12.69	1.03	0.11	0.36				
	South	983182	10.17	8	5.97	0.59	0.06	0.26				
	Southwest	968666	10.02	18	13.43	1.34	0.15	0.41				
	West	1001731	10.36	17	12.69	1.22	0.14	0.39				
	Northwest	1081116	11.18	16	11.94	1.07	0.12	0.36				
TWI	3.35–6.60	3709490	38.37	67	50.00	1.30	0.31	0.52	2.58	0.14	0.70	0.10
	6.61–8.31	2958038	30.60	39	29.10	0.95	0.23	0.49				
	8.32–10.6	1380575	14.28	18	13.43	0.94	0.22	0.48				
	10.7–13.2	1023657	10.59	6	4.48	0.42	0.10	0.33				
	13.3–16.9	507887	5.25	4	2.99	0.57	0.14	0.39				
	17.0–26.4	87129	0.90	0	0.00	0.00	0.00	0.00				
SPI	(−)13.8–−7.55	4159974	43.03	73	54.48	1.27	0.28	0.51	2.58	0.12	0.76	0.09
	(−)7.54–−3.79	552027	5.71	0	0.00	0.00	0.00	0.00				
	(−)3.78–−1.63	1973503	20.42	27	20.15	0.99	0.22	0.48				
	(−)1.62–0.424	1929918	19.96	23	17.16	0.86	0.19	0.45				
	(−)0.425–3.27	835865	8.65	9	6.72	0.78	0.17	0.44				
	3.28–15.2	215489	2.23	2	1.49	0.67	0.15	0.41				
Rainfall (mm)	514–909	5947911	61.53	86	64.18	1.04	0.28	0.51	2.58	0.55	0.63	0.35
	910–1480	2062529	21.34	27	20.15	0.94	0.25	0.50				
	1481–2220	904206	9.35	19	14.18	1.52	0.40	0.53				
	2221–3160	536944	5.55	2	1.49	0.27	0.07	0.27				
	3161–4620	146632	1.52	0	0.00	0.00	0.00	0.00				
	4621–6810	68554	0.71	0	0.00	0.00	0.00	0.00				

Continued on next page

Factors	Class	Class Pixels	Area (%)	Flood Pixels	Flood Area (%)	FR	(pij)	Hj	Hj max	lj	Pij	Wj
Distance from rivers (m)	0–433	2853230	29.52	91	67.91	2.30	0.68	0.38	2.58	0.59	0.57	0.33
	434–989	2909811	30.10	39	29.10	0.97	0.28	0.52				
	990–1590	2307000	23.87	4	2.99	0.13	0.04	0.18				
	1600–2010	896558	9.27	0	0.00	0.00	0.00	0.00				
	2020–2580	586509	6.07	0	0.00	0.00	0.00	0.00				
	2590–3940	113668	1.18	0	0.00	0.00	0.00	0.00				
Stream density (km/km^2)	0.1–0.847	2131227	22.05	0	0.00	0.00	0	0	2.58	0.36	1.95	0.70
	0.848–1.35	2391152	24.74	3	2.24	0.09	0.01	0.05				
	1.36–1.89	2149512	22.24	14	10.45	0.47	0.04	0.19				
	1.90–2.45	1603190	16.58	40	29.85	1.80	0.15	0.42				
	2.46–3.12	1034204	10.70	47	35.07	3.28	0.28	0.51				
	3.13–4.86	357491	3.70	30	22.39	6.05	0.52	0.49				
Soils Types	Vc	2956125	30.58	35	26.12	0.85	0.12	0.37	2.58	0.37	1.19	0.44
	Bv	1049119	10.85	60	44.78	4.13	0.58	0.46				
	Ap	970428	10.04	23	17.16	1.71	0.24	0.49				
	Lc	2516648	26.03	13	9.70	0.37	0.05	0.22				
	Vp	2042088	21.12	3	2.24	0.11	0.01	0.09				
	Ne	132368	1.37	0	0.00	0.00	0.00	0.00				
LULC	Water	295119	3.05	0	0.00	0.00	0.00	0.00	2.81	0.95	2.74	2.60
	Vegetation	600784	6.21	2	1.49	0.24	0.01	0.08				
	Flooded Vegetation	556	0.01	0	0.00	0.00	0.00	0.00				
	Agriculture	6806899	70.42	10	7.46	0.11	0.01	0.04				
	Built-up area	466702	4.83	122	91.04	18.86	0.98	0.03				
	Bare ground	1441	0.01	0	0.00	0.00	0.00	0.00				
	Hilly/Mountain area	1495275	15.47	0	0.00	0.00	0.00	0.00				
Distance from Road (m)	0–983	3136289	32.44	42	31.34	0.97	0.18	0.44	2.58	0.12	0.91	0.11
	984–2230	2794118	28.90	42	31.34	1.08	0.20	0.46				
	2240–3740	1942794	20.10	19	14.18	0.71	0.13	0.38				
	3750–5500	1271655	13.15	21	15.67	1.19	0.22	0.48				
	5510–9570	477445	4.94	10	7.46	1.51	0.28	0.51				
	9580–16700	44475	0.46	0	0	0	0.00	0.00				

3.3. Flood investigation by the SE model

The entropy values for eleven FCFs were calculated, and the results are summarized in Table 3. Based on the relationship between elevation and entropy values, the basin area with elevations between 436 and 565 meters had a higher likelihood of flooding than areas at higher elevations (Table 3). Khosravi et al. [56] stated that higher altitudes receive the most precipitation and that the possibility

of flooding is much lower in this region. Similar observations were reported by Manfreda et al. [67], and Pawar and Irfan [41]. The slope angle class of 2.84°–5.67° had the highest flood susceptibility in the Ghataprabha Basin. Runoff permeability and velocity were significantly correlated with surface slope (Table 3). According to Rahmati et al. [53], the likelihood of flooding in areas with low slope angles is low. The relationship between aspects and floods revealed that southwest, west, and east-facing areas are more likely to flood, and the maximum number of flood sites was associated with these aspects (Table 3). The highest P_{ij} value (0.31) was observed for the TWI class 3.35–6.60. It exhibited the highest flooding risk in areas, where TWI ranged from 3.35 to 6.60. Abdel Hamid et al. [68] reported that TWI indicates soil moisture levels in a given region and is used to detect areas prone to flooding (Table 3). The overall spatial distribution of TWI typically indicates potential flooding or saturation across the basin [56]. The SPI and entropy results indicated that the basin is most likely to flood when stream power is low. The uppermost P_{ij} value (0.28) observed for the SPI class ranged from −13.8 to −7.55 (Table 3). The maximum number of flood sites (86) was observed in the rainfall region, with rainfall ranging from 514 mm to 909 mm. For rainfall class 514–909 mm, the P_{ij} value was 0.28 (Table 3). This revealed that low-rainfall areas are more susceptible to flooding because they receive more runoff from higher-rainfall areas. The highest P_{ij} value, 0.68, was observed for locations within 0–433 m of rivers. This finding suggests that settlements adjacent to riverbanks are more vulnerable to flooding than those farther from rivers (Table 3). In addition, areas close to rivers are more likely to experience flooding [5]. The findings on stream density and flooding showed that a maximum P_{ij} value of 0.0.52 is associated with a density class of 3.13–4.86 km/km^2. This indicates that a higher stream density is associated with a higher risk of flooding in the area (Table 3). The highest reported Pij value, 0.58, was associated with the Bv soil type. The maximum number of flood sites (60) was observed in the Bv soil type region. The higher moisture retention capacity of Bv soil, compared with other soil types in the Ghataprabha Basin, is the primary factor contributing to its increased susceptibility to flooding (Table 3). The analysis of the LULC factor regarding flooding revealed that built-up areas (P_{ij} = 0.98) face the highest flood risk due to their reduced permeability and increased runoff (Table 3). Pawar et al. [5] found that the non-porous characteristics of surfaces in residential neighborhoods contribute to greater surface runoff and lower water infiltration. The maximum recorded value of P_{ij} was associated with the road distance interval of 5510–9570 m, indicating a low flood vulnerability. Compared with the other road distance classes, the 984-2230 m and 2240–3740 m classes had the highest number of flood-affected sites (42), indicating the highest likelihood of flood hazard (Table 3). The SE model facilitated flood-susceptibility prediction by assigning weightings (W_j) to each of the 11 Flood Contributing Factors (FCFs). The analysis of these weightings indicated that land use/land cover (2.60), stream density (0.70), soil types (0.44), rainfall (0.35), and distance from rivers (0.33) are the primary factors influencing flood risk in the basin. In contrast, the lowest weight (0.01) was assigned to the surface aspect factor, highlighting its negligible role in determining flood susceptibility within the Ghataprabha Basin (Table 3). Similar findings were noted by Pawar et al. [5]. Finally, the FSM was developed from the SE model results and subsequently categorized into five distinct flood-susceptibility zones, similar to the FR model (Figure 8a). The analysis from the SE model indicated that approximately 28% of the basin area is classified as very high flood vulnerability, whereas 35% falls within the high flood susceptibility category (Figure 8b). In contrast, it was indicated that the very low and low flood susceptibility zones account for only 3% and 11% of the area, respectively. Moreover, it was revealed that 23% of the

basin area falls within a moderate flood-vulnerability zone (Figure 8b). Figure 9 indicates some photographs of flooding that occurred in the Ghataprabha River in August 2019.

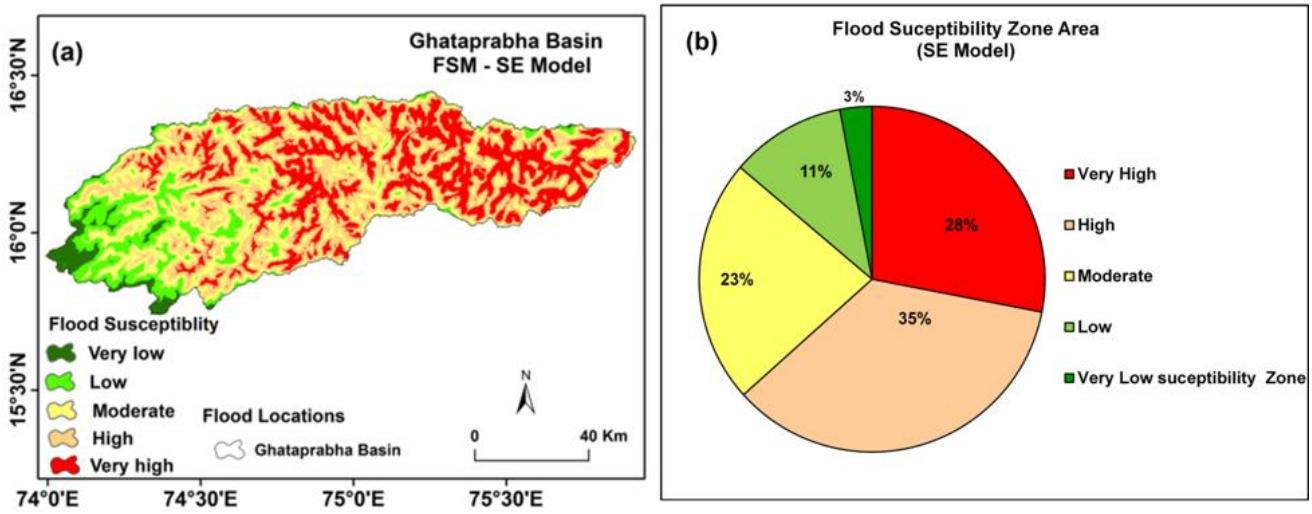


Figure 8. Flood susceptibility results from the SE Model.

3.4. Validation and comparison of flood models

The most crucial stage in any risk likelihood modeling process is validating the outcomes of the many models used. The results of the Flood susceptibility models have been validated using success and prediction rates [5,20]. The ROC was used to obtain the AUC for the training data (prediction rate) and the test data (success rate) for both models (Figure 10a, b). The success rate curves illustrated in Figure 10a and 10b assess the predictive effectiveness of the flood susceptibility model using the training dataset. This curve was created by plotting the cumulative percentage of recorded flood locations against the cumulative percentage of the study area, ranked from the highest to the lowest flood susceptibility values. The area under the receiver operating characteristic (ROC) curve (AUC) measures the model's ability to accurately identify flood-prone regions. An AUC value above 80% indicates exceptional predictive performance [41]. Thus, the high success rate shown in Figure 10b illustrates that the model successfully captures the spatial distribution of historical flood events. The AUC analysis showed that the FR Model had a success rate of 77.70% and a prediction rate of 70.83% (Figure 10a). The SE Model had a success rate of 84.99% and a prediction rate of 84.89% (Figure 10b). Therefore, ROC-AUC-based comparisons (FR and SE models) revealed that the SE model is more accurate for identifying flood-prone areas in the Ghataprabha Basin. Similar outcomes were reported by Arora et al. [69] and Chetia and Paul [70]. Sharma et al. [19] stated that Shannon's Entropy model is superior to the Frequency Ratio model while studying the flood susceptibility in the Chandrapur district of Maharashtra in India.





Destruction by Ghataprabha in Gokak Town during the August 2019 Flood. Photo: Abhay Kanvinde



Ghataprabha downstream Hidkal Barrage, August 2019. Photo: Abhay Kanvinde



Ghataprabha River at Gokak Falls, August 2019. Photo: Abhay Kanvinde



Ghataprabha River waters gushed into Gokak village. Credit: Deccan Herald Photo

Figure 9. Clips depicting the flood event of the Ghataprabha River that occurred in August 2019.

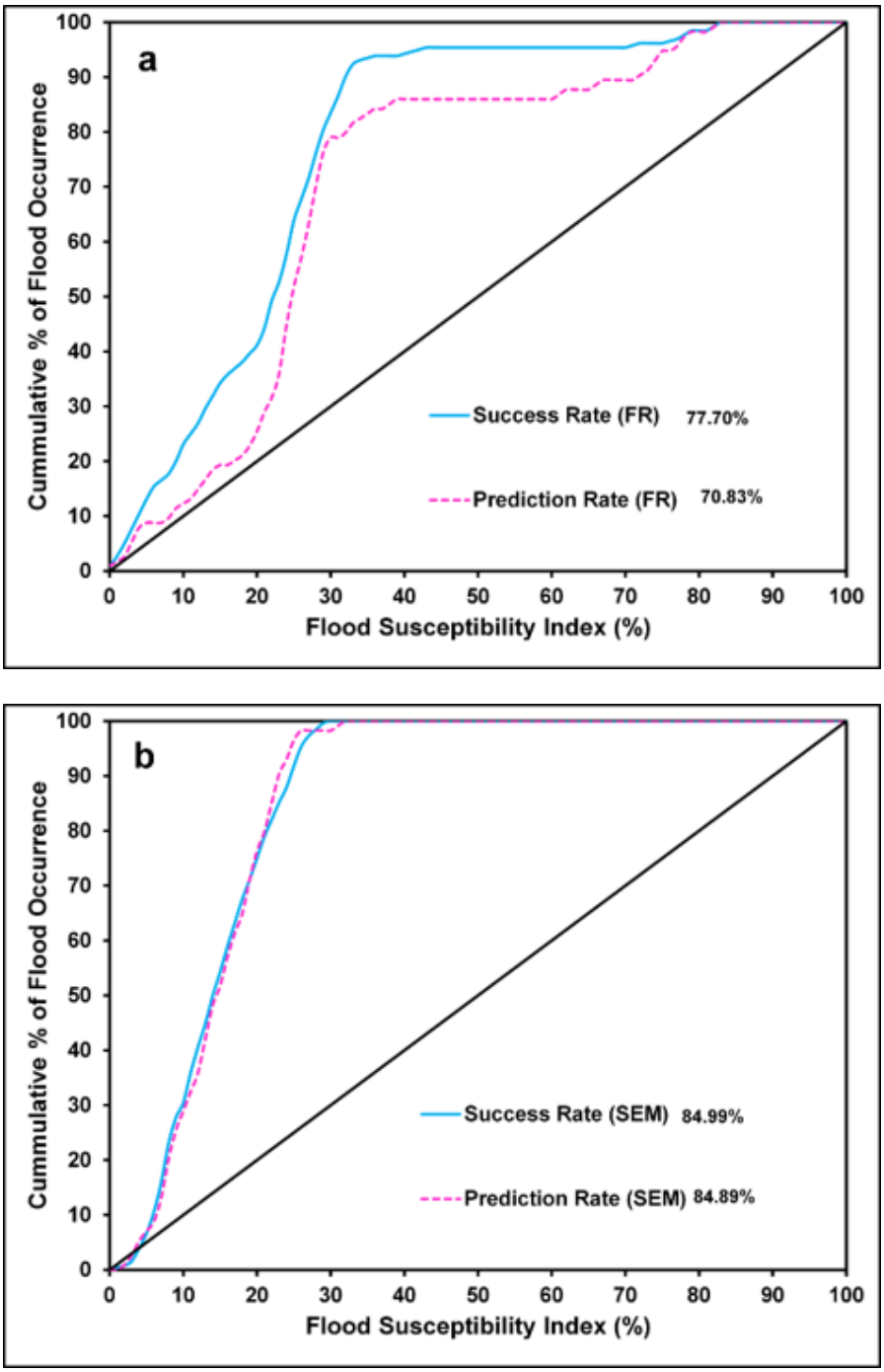


Figure 10. a Flood susceptibility FR model success and prediction rates by ROC-AUC b. Flood susceptibility SE model success and prediction rates by ROC-AUC.

4. Conclusions

The Ghataprabha River and its tributaries originate in the Western Ghats, a region that receives the highest rainfall during the monsoon season. Additionally, extreme rainfall events associated with monsoon lows often lead to flooding, particularly in the basin's low-lying areas. Therefore, accurate maps for assessing and managing flood risks are essential for flood-prone areas within the basin. The FR and SE models were applied to examine flood vulnerability. We used 11 FCFs to create a flood-

potential risk map for the Ghataprabha Basin. Among the eleven factors considered, the most noteworthy contributors to floods in the basin are built-up area, stream density, soil types, rainfall, and distance from rivers. Both models indicated success and prediction rates greater than 75%. The SE model achieved the highest success (84.99%) and prediction (84.89%) rates among the models. The SE model indicated that 28% of the basin area falls in the very high flood risk zone, while only 3% falls in the very low flood risk zone. Consequently, the results of the FSA derived from the SE model are deemed more accurate and beneficial for flood risk assessment and management within the Ghataprabha Basin. Our innovation lies in incorporating an extensive array of flood conditioning factors into the modeling of flood susceptibility. By validating the independence of predictor variables using Pearson's correlation analysis, the research reduces redundancy, strengthens model reliability, and establishes a reproducible GIS-based framework for evaluating flood susceptibility. This strategy provides a statistically valid basis for applying the frequency ratio and Shannon's Entropy models, supporting evidence-based flood risk management in river basins where data are scarce. Additionally, the generated FSM may help as a crucial tool for various decision-making processes connected to flood hazard management in the Ghataprabha Basin.

Author contributions

U.P: conceptualization, data processing, analysis and interpretation; K.K: introduction, methodology and result validation; U.R: supervision, review and editing, proofreading of the manuscript and technical inputs; N.M: review and editing, and final approval of the manuscript.

Use of AI tools declaration

The authors declare they have not used Artificial Intelligence (AI) tools in the creation of this article.

Acknowledgments

This study did not receive any funding.

Conflict of interest

The authors declare no conflicts of interest.

References

1. Tudose NC, Ungurean C, Davidescu Ș, et al. (2020) Torrential flood risk assessment and environmentally friendly solutions for small catchments located in the Romania Natura 2000 sites Ciucas, Postavaru and Piatra Mare. *Sci Total Environ* 698: 134271. https://doi.org/10.1016/j.scitotenv.2019.134271
2. Pawar U, Try S, Muttil N, et al. (2023) Frequency and trend analyses of annual peak discharges in the Lower Mekong Basin. *Heliyon* 9: e19690. https://doi.org/10.1016/j.heliyon.2023.e19690

3. Ibrahim M, Huo A, Ullah W, et al. (2024) Flood vulnerability assessment in the flood prone area of Khyber Pakhtunkhwa, Pakistan. *Front Environ Sci* 12: 1303976. https://doi.org/10.3389/fenvs.2024.1303976
4. Rentschler J, Salhab M, Jafino BA (2022) Flood exposure and poverty in 188 countries. *Nat Commun* 13: 3527. https://doi.org/10.1038/s41467-022-30727-4
5. Pawar U, Suppawimut W, Muttil N, et al. (2022) A GIS-Based Comparative Analysis of Frequency Ratio and Statistical Index Models for Flood Susceptibility Mapping in the Upper Krishna Basin, India. *Water* 14: 3771. https://doi.org/10.3390/w14223771
6. Kaya CM, Derin L (2023) Parameters and methods used in flood susceptibility mapping: a review. *J Water Clim Change* 14: 1935–1960. https://doi.org/10.2166/wcc.2023.035
7. Kurugama KM, Kazama S, Hiraga Y, et al. (2024) A comparative spatial analysis of flood susceptibility mapping using boosting machine learning algorithms in Rathnapura, Sri Lanka. *J Flood Risk Manag* 17: e12980. https://doi.org/10.1111/jfr3.12980
8. United Nations Office for Disaster Risk Reduction, Sendai Framework for Disaster Risk Reduction 2015–2030, 2015.
9. Saleh A, Yuzir A, Abustan I (2020) Flash Flood Susceptibility Modelling: A Review. *IOP Conference Series: Materials Science and Engineering,* 712: 012005.
10. Khouz A, Trindade J, Santos PP, et al. (2023) Flood Susceptibility Assessment through Statistical Models and HEC-RAS Analysis for Sustainable Management in Essaouira Province, Morocco. *Geosciences* 13: 382. https://doi.org/10.3390/geosciences13120382
11. Seleem O, Heistermann M, Bronstert A (2021) Efficient hazard assessment for pluvial floods in urban environments: A benchmarking case study for the city of Berlin, Germany. *Water* 13: 2476. https://doi.org/10.3390/w13182476
12. Yin D, Evans B, Wang Q, et al. (2020) Integrated 1D and 2D model for better assessing runoff quantity control of low impact development facilities on community scale. *Sci Total Environ* 720: 137630. https://doi.org/10.1016/j.scitotenv.2020.137630
13. Yariyan P, Avand M, Abbaspour RA, et al. (2020) Flood susceptibility mapping using an improved analytic network process with statistical models. *Geomat Nat Hazards Risk* 11: 2282–2314. https://doi.org/10.1080/19475705.2020.1836036
14. Msabi MM, Makonyo M (2021) Flood susceptibility mapping using GIS and multi-criteria decision analysis: A case of Dodoma region, central Tanzania. *Remote Sens Appl* 21: 100445. https://doi.org/10.1016/j.rsase.2020.100445
15. Salvati A, Nia AM, Salajegheh A, et al. (2023) Flood susceptibility mapping using support vector regression and hyper-parameter optimization. *J Flood Risk Manag* 16: e12920. https://doi.org/10.1111/jfr3.12920
16. Schmidt L, Heße F, Attinger S, et al. (2020) Challenges in Applying Machine Learning Models for Hydrological Inference: A Case Study for Flooding Events Across Germany. *Water Resour Res* 56: e2019WR025924. https://doi.org/10.1029/2019WR025924
17. Rudra RR, Sarkar SK (2023) Artificial neural network for flood susceptibility mapping in Bangladesh. *Heliyon* 9: e16459. https://doi.org/10.1016/j.heliyon.2023.e16459
18. Pradhan B, Lee S, Dikshit A, et al. (2023) Spatial flood susceptibility mapping using an explainable artificial intelligence (XAI) model. *Geosci Front* 14: 101625. https://doi.org/10.1016/j.gsf.2023.101625

19. Sharma A, Poonia M, Rai, A, et al. (2024) Flood Susceptibility Mapping Using GIS-Based Frequency Ratio and Shannon's Entropy Index Bivariate Statistical Models: A Case Study of Chandrapur District, India. *ISPRS Int J Geo-Inf* 13: 297. https://doi.org/10.3390/ijgi13080297
20. Tehrany MS, Kumar L, Neamah Jebur M, et al. (2019) Evaluating the application of the statistical index method in flood susceptibility mapping and its comparison with frequency ratio and logistic regression methods. *Geomat Nat Haz Risk* 10: 79–101. https://doi.org/10.1080/19475705.2018.1506509
21. Cao C, Xu P, Wang Y, et al. (2016) Flash flood hazard susceptibility mapping using frequency ratio and statistical index methods in coalmine subsidence areas. *Sustainability* 8: 948. https://doi.org/10.3390/su8090948
22. Tehrany MS, Shabani F, Jebur MN, et al. (2017) GIS-based spatial prediction of flood prone areas using standalone frequency ratio, logistic regression, weight of evidence and their ensemble techniques. *Geomat Nat Haz Risk* 8: 1538–1561. https://doi.org/10.1080/19475705.2017.1362038
23. Samanta S, Pal DK, Palsamanta B (2018) Flood susceptibility analysis through remote sensing, GIS and frequency ratio model. *Appl Water Sci* 8: 66. https://doi.org/10.1007/s13201-018-0710-1
24. Suppawimut W (2021) GIS-based flood susceptibility mapping using statistical index and weighting factor models. *Environ Nat Resour J* 19: 481–93. https://doi.org/10.32526/ENNRJ/19/2021003
25. Tehrany MS, Pradhan B, Mansor S, et al. (2015) Flood susceptibility assessment using GIS-based support vector machine model with different kernel types. *Catena* 125: 91–101. https://doi.org/10.1016/j.catena.2014.10.017
26. Mojaddadi H, Pradhan B, Nampak H, et al. (2017) Ensemble machine-learning-based geospatial approach for flood risk assessment using multi-sensor remote-sensing data and GIS. *Geomat Nat Haz Risk* 8: 1080–1102. https://doi.org/10.1080/19475705.2017.1294113
27. Sharma S, Kumari S (2024) Comparison of machine learning models for flood forecasting in the Mahanadi River Basin, India. *J Water Clim Change* 15: 1629–1652. https://doi.org/10.2166/wcc.2024.517
28. Kia MB, Pirasteh S, Pradhan B, et al. (2011) An artificial neural network model for flood simulation using GIS: Johor River Basin, Malaysia. *Environ Earth Sci* 67: 251–264. https://doi.org/10.1007/s12665-011-1504-z
29. Debnath J, Debbarma J, Debnath A, et al. (2024) Flood susceptibility assessment of the Agartala Urban Watershed, India, using machine learning algorithm. *Environ Monit Assess* 196: 110. https://doi.org/10.1007/s10661-023-12240-3
30. Aydin HE, Iban MC (2023) Predicting and analyzing flood susceptibility using boosting-based ensemble machine learning algorithms with SHapley Additive exPlanations. *Nat Hazards* 116: 2957–2991. https://doi.org/10.1007/s11069-022-05793-y
31. Asrade T, Abebe S, Tadesse K. et al. (2026) Flood susceptibility assessment using three machine learning techniques and comparison of their performance. *Sci Rep* 16: 8099. https://doi.org/10.1038/s41598-026-38391-0
32. Arora A, Arabameri A, Pandey M, et al. (2021) Optimization of state-of-the-art fuzzy-metaheuristic ANFIS-based machine learning models for flood susceptibility prediction mapping in the Middle Ganga Plain, India. *Sci Total Environ* 750: 1–20. https://doi.org/10.1016/j.scitotenv.2020.141565

33. NITI Aayog, Report of the Committee Constituted for Formulation of Strategy for Flood Management Works in Entire Country and River Management Activities and Works Related to Border Areas, 2021. Available from: https://www.niti.gov.in/sites/default/files/2023-02/Flood-Report.pdf.
34. Central Water Commission (CWC), *Water Year Book*, Vol I, Discharge Year Book. Hyderabad, 1-689P. 2021. Available from: https://www.cwc.gov.in/en/water-year-books.
35. Pathak AA, Dodamani BM (2020) Trend analysis of rainfall, rainy days and drought: a case study of Ghataprabha River Basin, India. *Model Earth Syst Environ* 6: 1357–1372. https://doi.org/10.1007/s40808-020-00798-7
36. Ullah K, Zhang J (2020) GIS-based flood hazard mapping using relative frequency ratio method: A case study of Panjkora River Basin, eastern Hindu Kush, Pakistan. *PLoS One* 15: e0229153. https://doi.org/10.1371/journal.pone.0229153
37. Majeed M, Lu L, Anwar MM, et al. (2023) Prediction of flash flood susceptibility using integrating analytic hierarchy process (AHP) and frequency ratio (FR) algorithms. *Front Environ Sci* 10: 1037547.
38. Pawar U (2025) An identification and mapping of flood susceptible areas in the Wardha Basin using frequency ratio and statistical index models, India. *Environ Sci Pollut Res* 32: 1565–1580. https://doi.org/10.1007/s11356-024-35871-6
39. Merz B, Thieken AH, Gocht M (2007) Flood risk mapping at the local scale: concepts and challenges, *lood Risk Management in Europe. Advances in Natural and Technological Hazards Research*, vol 25, Springer, Dordrecht, 231–251. https://doi.org/10.1007/978-1-4020-4200-3_13
40. Klemes V (1986) Operational testing of hydrological simulation models. *Hydrol Sci J* 31: 13–24. https://doi.org/10.1080/02626668609491024
41. Pawar U, Irfan M (2026) Integrating Flood Control Factors for Enhanced Flood Risk Modeling: A Study of the Malaprabha Basin Through Frequency Ratio and Statistical Index Approaches, In: Ghosh S, Eds., *Reimagining Indian Rivers for Sustainability*. *Palgrave Studies in Environmental Sustainability*, Palgrave Macmillan, Cham. https://doi.org/10.1007/978-3-032-04754-0_21
42. Fernandez DS, Lutz MA (2010) Urban flood hazard zoning in Tucumán Province, Argentina, using GIS and multicriteria decision analysis. *Eng Geol* 111: 90–98. https://doi.org/10.1016/j.enggeo.2009.12.006
43. Rahman M, Ningsheng C, Islam MM, et al. (2019) Flood susceptibility assessment in Bangladesh using machine learning and multi-criteria decision analysis. *Earth Syst Environ* 3: 585–601. https://doi.org/10.1007/s41748-019-00123-y
44. Bathrellos GD, Skilodimou HD, Soukis K, et al. (2018) Temporal and spatial analysis of flood occurrences in the drainage basin of Pinios river (Thessaly, Central Greece). *Land* 7: 106. https://doi.org/10.3390/land7030106
45. Malaperdas GD, Panagiotidis VV (2018) The aspects of Aspect: Understanding land exposure and its part in geographic information systems analysis. *Energy Environ* 29: 1022–1037. https://doi.org/10.1177/0958305X18766322
46. Moore ID, Grayson RB, Ladson AR (1991) Digital terrain modeling: a review of hydrological, geomorphological and biological applications. *Hydrol Process* 5: 3–30. https://doi.org/10.1002/hyp.3360050103

47. Jebur MN, Pradhan B, Tehrany MS (2014) Optimization of landslide conditioning factors using very high-resolution airborne laser scanning (LiDAR) data at catchment scale. *Remote Sens Environ* 152:150–165. https://doi.org/10.1016/j.rse.2014.05.013
48. Wang N, Sun F, Koutsoyiannis D, et al. (2023) How can changes in the human-flood distance mitigate flood fatalities and displacements? *Geophys Res Lett* 50: e2023GL105064. https://doi.org/10.1029/2023GL105064
49. Horton RE (1945) Erosional development of streams and their drainage basins; hydrophysical approach to quantitative morphology. *Geol Soc Am Bull* 56: 275–370. https://doi.org/10.1130/0016-7606(1945)56[275:EDOSAT]2.0.CO;2
50. Das S (2019) Geospatial mapping of flood susceptibility and hydro-geomorphic response to the floods in Ulhas Basin, India. *Remote Sens Appl* 14: 60–74. https://doi.org/10.1016/j.rsase.2019.02.006
51. Pawar U, Suppawimut W, Rathnayake U (2024) Mapping of groundwater potential zones in a drought prone Marathwada Region using frequency ratio and statistical index methods, India. *Results Eng* 22:101994. https://doi.org/10.1016/j.rineng.2024.101994
52. Alaghmand S, Beecham S, Hassanli A (2014) Impacts of vegetation cover on surface-groundwater flows and solute interactions in a semi-arid saline floodplain: a case study of the lower Murray River, Australia. *Environ Process* 1: 59–71. https://doi.org/10.1007/s40710-014-0003-0
53. Rahmati O, Pourghasemi HR, Zeinivand H (2016) Flood susceptibility mapping using frequency ratio and weights-of-evidence models in the Golastan Province, Iran. *Geocarto Int* 31: 42–70. https://doi.org/10.1080/10106049.2015.1041559
54. Sahana M, Rehman S, Sajjad H, et al. (2020) Exploring effectiveness of frequency ratio and support vector machine models in storm surge flood susceptibility assessment: a study of Sundarban Biosphere Reserve, India. *Catena* 189: 104450. https://doi.org/10.1016/j.catena.2019.104450
55. Shannon CE (1948) A mathematical theory of communication. *Bell Syst Tech J* 27: 379–423. https://doi.org/10.1002/j.1538-7305.1948.tb01338.x
56. Khosravi K, Pourghasemi HR, Chapi K, et al. (2016) Flash flood susceptibility analysis and its mapping using different bivariate models in Iran: a comparison between Shannon's entropy, statistical index, and weighting factor models. *Environ Monit Assess* 188: 656. https://doi.org/10.1007/s10661-016-5665-9
57. Haghizadeh A, Siahkamari S, Haghiabi AH, et al. (2017) Forecasting flood-prone areas using Shannon's entropy model. *J Earth Syst Sci* 126: 39. https://doi.org/10.1007/s12040-017-0819-x
58. Arabameri A, Pal SC, Rezaie F, et al. (2021) Comparison of multi-criteria and artificial intelligence models for land-subsidence susceptibility zonation. *J Environ Manage* 284: 112067. https://doi.org/10.1016/j.jenvman.2021.112067
59. Lee S, Kim YS, Oh HJ (2012) Application of a weights-of-evidence method and GIS to regional groundwater productivity potential mapping. *J Environ Manage* 96: 91–105. https://doi.org/10.1016/j.jenvman.2011.09.016
60. Tehrany MS, Pradhan B, Jebur MN (2013) Spatial prediction of flood susceptible areas using rule-based decision tree (DT) and a novel ensemble bivariate and multivariate statistical models in GIS. *J Hydrol* 504: 69–79. https://doi.org/10.1016/j.jhydrol.2013.09.034

61. Khosravi K, Nohani E, Maroufinia E, et al. (2016) A GIS-based flood susceptibility assessment and its mapping in Iran: a comparison between frequency ratio and weights-of-evidence bivariate statistical models with multi-criteria decision-making technique. *Nat Hazards* 83: 947–987. https://doi.org/10.1007/s11069-016-2357-2
62. Chapi K, Singh VP, Shirzadi A, et al. (2017) A novel hybrid artificial intelligence approach for flood susceptibility assessment. *Environ Modell Softw* 95: 229–245. https://doi.org/10.1016/j.envsoft.2017.06.012
63. Seebauer S, Winkler C (2020) Should I stay or should I go? Factors in household decisions for or against relocation from a flood risk area. *Global Environ Chang* 60: 102018. https://doi.org/10.1016/j.gloenvcha.2019.102018
64. Onuşluel Gül G (2013) Estimating flood exposure potentials in Turkish catchments through index-based flood mapping. *Nat Hazards* 69: 403–423. https://doi.org/10.1007/s11069-013-0717-8
65. Youssef AM, Pradhan B, Sefry SA (2016) Flash flood susceptibility assessment in Jeddah city (Kingdom of Saudi Arabia) using bivariate and multivariate statistical models. *Environ Earth Sci* 75: 1–16. https://doi.org/10.1007/s12665-015-4830-8
66. Shahabi H, Shirzadi A, Ronoud S, et al. (2021) Flash flood susceptibility mapping using a novel deep learning model based on deep belief network, back propagation and genetic algorithm. *Geosci Front* 12: 101100. https://doi.org/10.1016/j.gsf.2020.10.007
67. Manfreda S, Di Leo M, Sole A (2011) Detection of flood-prone areas using digital elevation models. *J Hydrol Eng* 16: 781–790. https://doi.org/10.1061/(asce)he.1943-5584.0000367
68. Abdel Hamid HT, Wenlong W, Qiaomin L (2020) Environmental sensitivity of flash flood hazard using geospatial techniques. *Global J Environ Sci Manage* 6: 31–46. https://doi.org/10.22034/gjesm.2020.01.03
69. Arora A, Pandey M, Siddiqui MA, et al. (2019) Spatial flood susceptibility prediction in Middle Ganga Plain: comparison of frequency ratio and Shannon's entropy models. *Geocarto Int* 36: 2085–2116. https://doi.org/10.1080/10106049.2019.1687594
70. Chetia L, Paul SK (2024) Spatial Assessment of Flood Susceptibility in Assam, India: A Comparative Study of Frequency Ratio and Shannon's Entropy Models. *J Indian Soc Remote Sens* 52: 343–358. https://doi.org/10.1007/s12524-023-01798-7



AIMS Press

© 2026 the Author(s), licensee AIMS Press. This is an open access article distributed under the terms of the Creative Commons Attribution License (http://creativecommons.org/licenses/by/4.0)